ACS Photonics

pubs.acs.org/journal/apchd5

Article

Quantum Emission Assisted by Energy Landscape Modification in Pentacene-Decorated Carbon Nanotubes

Zhen Li,* Keigo Otsuka, Daiki Yamashita, Daichi Kozawa, and Yuichiro K. Kato*

Cite This: *ACS Photonics* 2021, 8, 2367−2374

Read Online

ACCESS | Metrics & More | Article Recommendations | Supporting Information

ABSTRACT: Photoluminescent carbon nanotubes are expected to become versatile single-photon sources that have applications in quantum information processing. Quantum emission from carbon nanotubes is often induced by localization of excitons or exciton−exciton annihilation. Here, we modify the local energy landscape of excitons by decorating nanoscale pentacene particles onto air-suspended single-walled carbon nanotubes. Directional exciton transfer from the undecorated region to the decorated site is demonstrated, suggesting exciton trapping induced by local dielectric screening from pentacene particles. Photoluminescence and photon correlation measurements on a representative carbon nanotube reveal enhanced exciton−exciton annihilation and single-photon emission at room temperature. Pentacene particles are shown to promote strong photon antibunching at the decorated site, indicating that noncovalent functionalization using molecules can be an effective approach for energy landscape modification and quantum emission in carbon nanotubes.

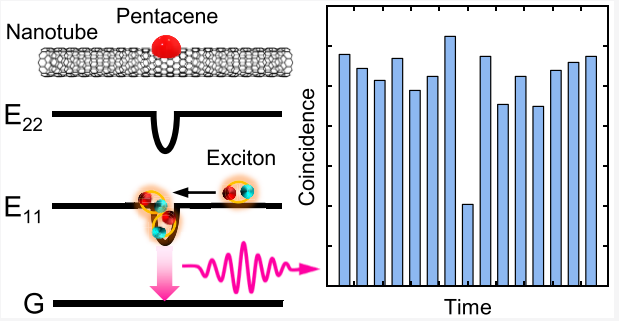

KEYWORDS: *carbon nanotubes, organic molecules, photoluminescence, excitons, single-photon sources, dielectric engineering*

Single-photon sources are a crucial component for quantum information processing and quantum key distribution,[1−5] and relentless research efforts have been made to pursue the ideal material platform.[6−22] In recent years, semiconducting single-walled carbon nanotubes (CNTs) have emerged as promising candidates for single-photon sources because of their stable excitonic states at room temperature[23,24] and photoluminescence (PL) wavelengths in the telecommunication range.[25,26] Due to limited screening of the Coulomb interaction in the unique one-dimensional structure, tightly bound electron−hole pairs form excitons that exhibit fast diffusion along the CNT axis.[26−32] In most cases, exciton diffusion in a typical CNT leads to spreading of the exciton population along the CNT axis that gives rise to multiphoton emission, while nonradiative recombination predominantly occurs at the quenching sites between the CNT and the substrate.[31,33]

To enhance photon antibunching and generate single photons from the excitons in CNTs, proper control of the exciton diffusion is necessary. One commonly adopted approach is the exciton localization. Free excitons in covalently functionalized CNTs can be captured at defect-induced deep trapping states, where PL brightening,[34−37] high-purity single-photon emission, and long exciton lifetimes have been achieved.[38−40] Furthermore, spontaneous localization of the band-edge excitons due to environmental disorders or unintentional molecular adsorption is also possible in undoped CNTs at cryogenic temperatures, where signatures of quantum correlation have been observed.[41−50] Alternatively, exciton−exciton annihilation (EEA) can be adopted to promote strong photon antibunching.[32,51] Single-photon emission at room temperature induced by the diffusion-driven EEA among spatially separated free excitons has been demonstrated in undoped air-suspended CNTs.[51]

An additional approach that can possibly control the exciton diffusion and induce strong photon antibunching is the noncovalent functionalization of CNTs by intentional molecular adsorption. Because of the atomically thin nature of CNTs, excitons in air-suspended CNTs are highly sensitive to the dielectric environment, and adsorbed molecules can cause a significant reduction in the excitonic energies.[52−61] Meanwhile, the excellent optical properties of the CNTs can be preserved because noncovalent functionalization is less perturbative, and the molecular coverage can be effectively controlled by different adsorption conditions or heating-induced molecular desorption.[53,54,57,60] To induce photon antibunching, a local potential well with a reduced excitonic energy can be created by adsorbing a nanoscale molecular

Received: April 8, 2021
Published: July 13, 2021

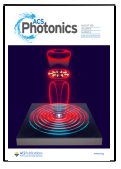

particle onto an air-suspended CNT. Although the potential dip induced by the molecule is expected to be shallow, it should be possible to guide the majority of the free excitons into the potential well and suppress multiphoton emission from spatially separated excitons in the pristine region. As a result of the high density of excitons in the potential well, efficient EEA should occur, and photon antibunching is expected.

By utilizing a type of versatile molecule, pentacene,[62−65] we demonstrate directional exciton transfer and room-temperature single-photon emission in air-suspended CNTs decorated with nanoscale pentacene particles. The pentacene particles are deposited onto individually suspended CNTs by thermal evaporation, where we observe pentacene decoration dependent on the CNT chiral angle. PL imaging and PL excitation (PLE) spectroscopy are performed on such CNTs, and additional peaks with redshifted emission energies are identified after pentacene decoration. Directional exciton transfer from the undecorated region to the decorated site is demonstrated by PLE spectroscopy on a representative CNT. Excitation-power-dependent PL spectra measured from different emission peaks reveal enhanced EEA at the decorated site, and the exciton trapping rate is calculated to be higher than the detrapping rate at room temperature. Single-photon emission from the redshifted emission peak at the decorated site on the representative CNT is also observed. Additional photon correlation measurements performed on more CNTs indicate that pentacene decoration is on average beneficial for stronger photon antibunching.

RESULTS AND DISCUSSION

Air-suspended CNTs are synthesized on trenched Si/SiO_2 substrates,[26] and pentacene is deposited onto the CNTs by thermal evaporation [Figure 1(a)]. After pentacene deposition, amorphous pentacene particles with diameters of tens of nanometers are decorated on the CNTs, as shown in Figure 1(b) and Supporting Figure S1. As the thickness of the deposited pentacene film is monitored during the deposition process, the approximate size of the particles can be quantitatively controlled by adjusting the deposition duration. In Figure 1(c), the decorated pentacene particle diameters measured in the scanning-electron microscope (SEM) images are plotted against the nominal thickness of the pentacene film on the substrate. Their relation follows a cube root fit

$$d = kt^{1/3} \quad (1)$$

where the coefficient $k = 30.7\ \mathrm{nm}^{2/3}$, d is the particle diameter, and t is the nominal pentacene film thickness. We note that the actual pentacene film thickness on the substrate is distributed nonuniformly, and there is a discrepancy between the actual film thickness and the nominal thickness (Supporting Figure S2). Nevertheless, the cube root relation is reasonably consistent.

The percentage of CNTs decorated with pentacene particles is determined from about 400 individually suspended CNTs (Supporting Information). As shown in Figure 1(d), pentacene decoration shows a dependency on the CNT species; namely, CNTs with chiral angles larger than 20° exhibit a greater probability to be decorated. While the randomly distributed defects on the CNTs such as amorphous carbon or other contaminants may serve as nuleation sites for pentacene, we speculate that the orientation of the pentacene molecule relative to that of the CNT has a major influence on the percentage of the pentacene-decorated CNTs. Density functional theory calculations[66] have demonstrated that the "bridge" configuration (six-membered rings of pentacene laying over the middle of the C−C bonds in a plane-to-plane configuration) in an armchair CNT (chiral angle 30°) is energetically favorable for pentacene adsorption, while CNTs with smaller chiral angles are less favorable due to the high curvature along the direction of this configuration.

Before pentacene decoration, automated PL line scans are performed throughout the trenches on the Si/SiO_2 substrate to locate bright CNTs, then selected CNTs are individually characterized in sequence by polarization-dependent PL, PLE spectroscopy, and PL imaging with a power $P = 10\ \mu$W. A PLE map obtained from a representative pristine CNT (Supporting Information) is shown in Figure 2(a). This CNT shows bright PL and a peak height of 11 680 counts/s, and we name this peak the "pristine peak". The E_{11} and E_{22} resonance energies are 0.954 and 1.598 eV, respectively. By comparing the resonance energies with tabulated data from air-suspended CNTs,[26] the chirality of this CNT is assigned to (9,7). In Figure 2(b), the PL intensities integrated over a 4 nm spectral window centered at the PL emission energy reveal that the CNT is individual and fully suspended with a length of approximately 3.3 μm.

Pentacene with a nominal film thickness of 2.8 nm is then deposited onto this sample after the initial PL characterization. Polarization-dependent PL intensity plots [insets of Figure 2(a) and (c)] are compared before and after pentacene decoration, which allows us to verify that the same CNT has been measured. In the PLE map taken at the pentacene particle, as shown in Figure 2(c), two prominent emission peaks are present. One peak has a peak height of 4416 counts/s, and E_{11} and E_{22} resonance energies at 0.953 and 1.596 eV, respectively. Since its resonance energies agree with that of the pristine peak, this peak should correspond to the excitons in

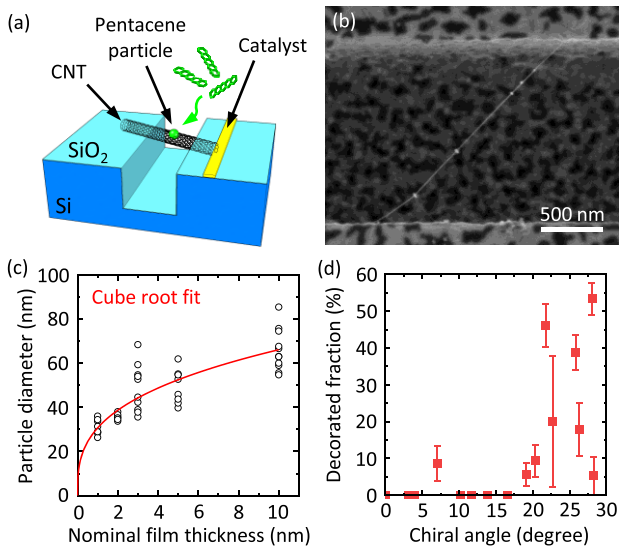

Figure 1. (a) Schematic showing pentacene adsorption onto an air-suspended CNT on a trenched Si/SiO_2 substrate. (b) SEM image of air-suspended CNTs decorated with pentacene particles. (c) Diameters of the decorated pentacene particles as a function of the nominal pentacene film thickness. Red curve is a cube root fit. (d) Percentage of CNTs decorated with pentacene particles with respect to the chiral angles.

https://doi.org/10.1021/acsphotonics.1c00539
ACS Photonics 2021, 8, 2367−2374

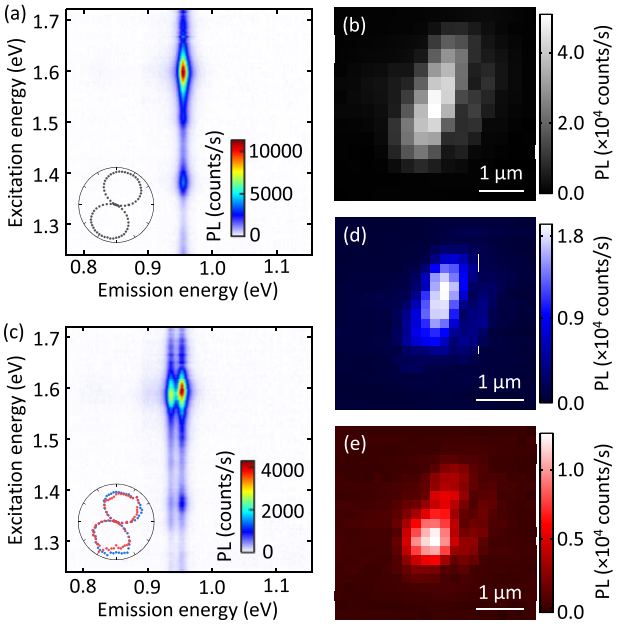

Figure 2. (a) PLE map of a typical (9,7) CNT before pentacene decoration. Inset shows the polarization-dependent integrated PL intensity of the pristine peak (black dots). (b) Integrated PL image of the pristine peak near 0.95 eV. (c) PLE map of the same CNT after pentacene decoration. Inset shows the polarization-dependent integrated PL intensities of the undecorated peak (blue dots) and decorated peak (red dots). Integrated PL images of (d) the undecorated peak near 0.95 eV and (e) decorated peak near 0.94 eV, respectively.

the undecorated region on the CNT and is termed the "undecorated peak". The slight redshifts compared to the pristine peak can be caused by fitting errors, while the thin molecular films adsorbed on the undecorated region (Supporting Figure S1) are also speculated to play a role. The additional peak introduced by pentacene decoration has a peak height of 2875 counts/s, and E_{11} and E_{22} resonance energies at 0.938 and 1.591 eV, respectively. Both resonance energies are redshifted compared to the pristine peak (ΔE_{11} = 16 meV, ΔE_{22} = 7 meV), and this peak is named the "decorated peak". Weaker peaks corresponding to the 2u state with excitation energies near 1.4 eV are also visible before and after pentacene decoration, which will be discussed later.

The total peak height of the two prominent peaks is about 62% of the original peak height in the pristine state, which could suggest efficient EEA and/or PL quenching induced by the adsorbed pentacene molecules. Nevertheless, the reduction in PL intensity is relatively weak compared to other molecular types that can induce charge transfer,[60] which is advantageous for exciton transfer and efficient EEA because long exciton lifetimes and high quantum efficiency can be preserved.

Since an additional emission peak appears after pentacene decoration, separate PL images can be obtained by integrating the PL intensities near emission energies of 0.953 and 0.938 eV, respectively [Figure 2(d) and (e)]. Based on the PL images, no significant strain is introduced after pentacene decoration as the shape of the CNT stays the same. The location of the decorated pentacene particle is found to be near the bottom of the CNT as shown in Figure 2(e).

On another (9,7) CNT decorated with pentacene from the same sample substrate, location-dependent PLE spectroscopy is performed [Figure 3(a)]. The PLE maps are taken from spot 1 to spot 6 along the axis of the CNT as marked by orange circles in the PL image in Figure 3(b). This CNT is decorated with one pentacene particle at the middle as shown in the PL image in Figure 3(c). We note that PL imaging may not be able to resolve multiple closely located pentacene particles since the beam spot size is approximately 1 μm. In the PLE map taken at spot 1, where the region is not decorated by the

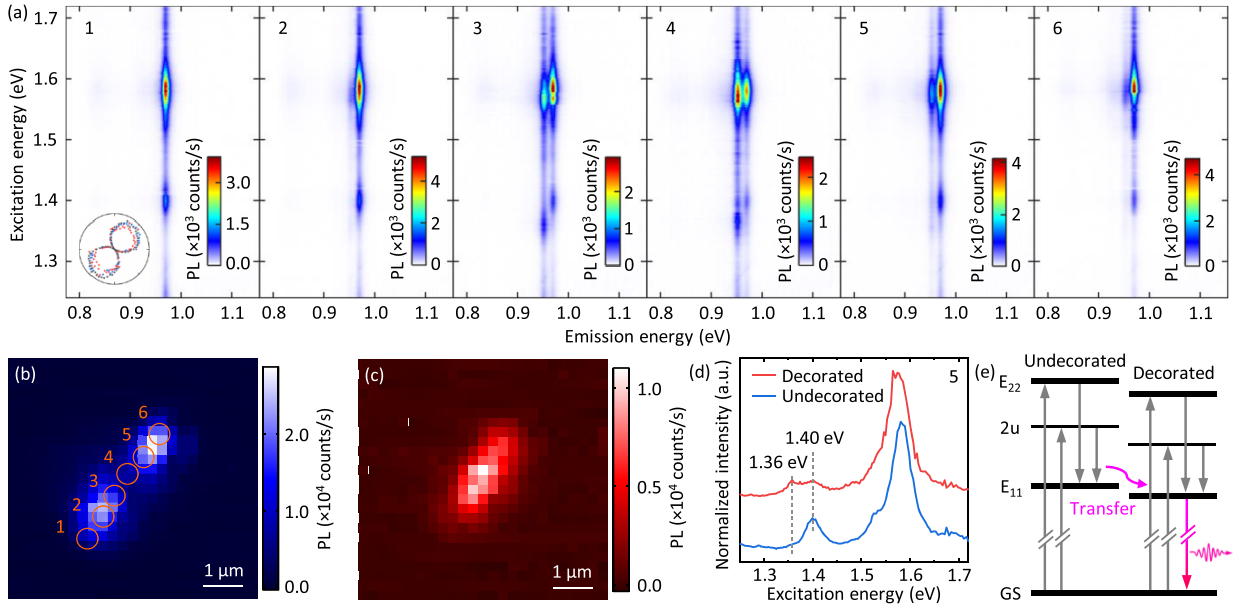

Figure 3. (a) PLE maps taken at spots 1–6 as marked in (b) along a (9,7) CNT decorated with pentacene. Inset contains the polarization-dependent integrated PL intensities of the pristine peak (black dots), undecorated peak (blue dots), and decorated peak (red dots), respectively. Integrated PL images of the (b) undecorated peak near 0.97 eV and (c) decorated peak near 0.95 eV. (d) Amplitude plot of the PLE spectra obtained by double Lorentzian fitting of the PLE map taken at spot 5. The red curve corresponds to the decorated peak, and the blue curve corresponds to the undecorated peak. (e) Energy level diagram showing the exciton transfer from the undecorated region to the decorated site.

https://doi.org/10.1021/acsphotonics.1c00539
ACS Photonics 2021, 8, 2367–2374

pentacene particle, there is a single undecorated peak with E_{11} and E_{22} resonance energies at 0.971 and 1.583 eV, respectively. While at spot 4, where the pentacene particle is decorated, two prominent peaks coexist in the PLE map: an undecorated peak with approximately the same energies (0.970 and 1.581 eV) as the peak observed at spot 1 and a decorated peak with redshifted E_{11} and E_{22} resonance energies at 0.953 and 1.575 eV, respectively. The redshift between the E_{11} resonance energies of the decorated and undecorated peaks at spot 4 is 17 meV, which also corresponds to the depth of the potential well created by pentacene, whereas the redshift between the E_{22} resonance energies is 6 meV. For a CNT under dielectric screening, the amount of redshift in both E_{11} and E_{22} resonance energies should be comparable.[25,61] Hence, the relatively small redshift in the E_{22} resonance energies of the pentacene-decorated CNTs cannot be explained by the simple picture of dielectric screening, and the transfer of excitons should be considered.

The effect of exciton transfer manifests in the behavior of the weaker 2u peaks. As shown in Figure 3(d), the PLE spectra obtained from the PLE map of spot 5 at emission energies corresponding to the undecorated and decorated peaks are depicted as blue and red curves, respectively. Contrary to typical CNTs under dielectric screening,[59,61] two 2u peaks are present in the decorated PLE spectrum: one 2u peak has a redshifted excitation energy at 1.358 eV that is induced by dielectric screening of pentacene; another 2u peak has an excitation energy of 1.398 eV that is consistent with the excitation energy 1.401 eV of the 2u peak in the undecorated PLE spectrum. The coexistence of the two 2u peaks in the decorated PLE spectrum is an indication of directional exciton transfer, and it can be explained by the energy diagram in Figure 3(e). Excitons at the 2u state are generated in the undecorated and decorated regions simultaneously under laser excitation. The excitons from the decorated site are at a lower 2u state due to dielectric screening, and they subsequently relax to the lower E_{11} state to recombine radiatively. Meanwhile, the excitons from the undecorated region are at a higher 2u state, and they transfer to the decorated site with a lower 2u state followed by radiative recombination from the same lower E_{11} state. This exciton transfer process gives rise to two 2u peaks with the same redshifted E_{11} resonance energy, but with a redshifted and an unshifted excitation energy. Furthermore, because no extra 2u peaks are observed in the undecorated PLE spectrum [Figure 3(d)], we conclude that the excitons predominantly transfer from the undecorated region to the decorated site. Likewise, in the presence of directional exciton transfer, one should also expect two E_{22} resonance peaks in the decorated PLE spectrum; however, only one redshifted peak is observed as previously mentioned. It has been reported that the redshift of the E_{22} resonance is two to three times smaller than that of the 2u peak in CNTs under dielectric screening,[67] and the less redshifted E_{22} resonance of the decorated peak is thus speculated to be the superposition of a E_{22} resonance with a redshifted energy more than 10 meV smaller than 1.583 eV (undecorated peak) due to dielectric screening (Supporting Figure S3) and an unshifted E_{22} resonance with an energy near 1.583 eV due to directional exciton transfer.

To understand the exciton dynamics in the pentacene-decorated CNTs, we perform excitation-power-dependent PL measurements at the particle [spot 4 in Figure 3(b)] on the same CNT where the directional exciton diffusion has been demonstrated. PL intensities as a function of the excitation power for each emission peak before and after pentacene decoration are shown in Figure 4(a). The curves corresponding to the pristine peak and the undecorated peak show a similar behavior throughout the power range, but the curve for the decorated peak deviates to a lower slope above 0.7 μW. It is known that the PL intensity and the excitation power follow a linear relationship at low power, and the relationship becomes sublinear at high powers due to EEA.[26] Hence, the early deviation of the decorated peak intensity at lower powers is a signature of more efficient EEA owning to higher density of excitons at the decorated site than in the undecorated region.

PL decay curves corresponding to the undecorated and decorated emission peaks are also measured at spot 4 by using a bandpass filter (Supporting Figure S4), and the exciton lifetimes are extracted from the PL decay curves by biexponential fitting convoluted with the instrument response function (IRF) [Figure 4(b)]. Two decay components are obtained in each PL decay curve: a fast component with a lifetime τ_1 associated with bright excitonic states that contribute significantly to the emission intensity, and a slow component with a lifetime τ_2 associated with dark excitonic states.[68−70] The difference between τ_1 of the undecorated and decorated peaks is not clearly distinguishable, which could be due to the fact that exciton trapping and detrapping occur faster than exciton recombination.[71] Fast exciton trapping and detrapping are also evidenced by the relatively bright decorated peak in the PLE map [Figure 3(a)] considering the small diameter of the pentacene particle (<100 nm) with respect to the 1 μm laser spot size. Supposedly, in a scenario where excitons recombine earlier than they engage in the trapping and detrapping process, the decorated peak intensity should

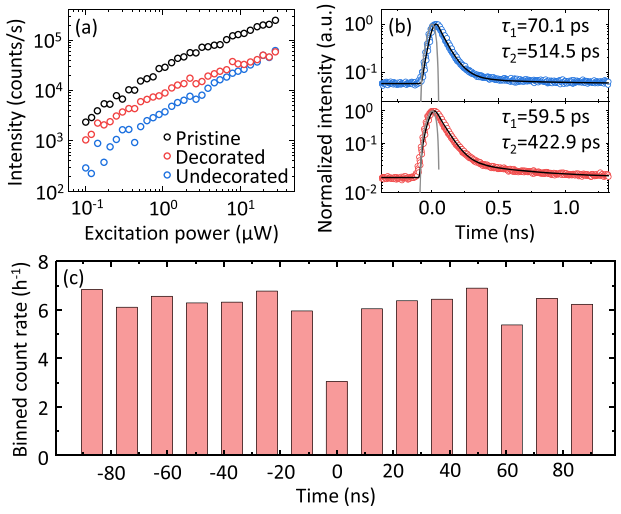

Figure 4. (a) Excitation power dependence of the PL intensities corresponding to the pristine peak (black circles), decorated peak (red circles), and undecorated peak (blue circles). The excitation energy is 1.59 eV. (b) PL decay curves (blue or red circles) taken at the pentacene-decorated site on the CNT using a bandpass filter. Top panel: undecorated peak at 0.97 eV. Bottom panel: decorated peak at 0.95 eV. The black curves are the biexponential fit, and the grey curves are the IRF. An excitation energy of 1.57 eV and pulsed P = 50 nW are used. (c) Binned count-rate histogram taken with an excitation energy of 1.57 eV and pulsed P = 10 nW at the pentacene-decorated site using a bandpass filter. The data in (c) are accumulated from measurements performed for 33 h in an ambient condition.

https://doi.org/10.1021/acsphotonics.1c00539
ACS Photonics 2021, 8, 2367−2374

become much weaker, since only a small number of excitons are excited at the nanoscale decorated site.

Finally, photon correlation measurements are conducted at the decorated site on this CNT in an ambient condition with the decorated emission peak isolated by the bandpass filter. The autocorrelation histogram is evaluated by subtracting the dark counts and binning each peak, as shown in the binned count-rate histogram in Figure 4(c). The zero-delay second-order intensity correlation $g^{(2)}(0)$ is obtained by calculating the ratio between the peak count at zero time delay and the average count of the other peaks. For this pentacene-decorated CNT, $g^{(2)}(0)$ is 0.48 at P = 10 nW, indicating single-photon emission at room temperature.

Quantitatively, the strength of exciton trapping by the pentacene particle can be evaluated from the ratio between the trapping rate and the detrapping rate. Assuming a single potential well is created by the pentacene particle on this CNT, and excitons can occupy either the decorated state or the undecorated state, the trapping rate to detrapping rate ratio is then determined by the Boltzmann factor as

$$\frac{k_{\text{trap}}}{k_{\text{detrap}}} = \exp\left(\frac{\Delta E}{k_B T}\right) \tag{2}$$

where ΔE is the energy difference between the undecorated state and the decorated state, k_B is the Boltzmann constant, and T is the temperature. Using ΔE = 17 meV as obtained from the PLE map in Figure 3(a), the ratio between the trapping rate and the detrapping rate at room temperature is 1.9. This suggests that the potential well created by pentacene can induce exciton trapping at room temperature.

Furthermore, the validity of our calculation can be verified by using the steady-state rate equation for excitons within the laser spot

$$g + k_{\text{detrap}}N^* - \frac{N}{\tau} - k_{\text{trap}}N = 0 \tag{3}$$

$$g^* + k_{\text{trap}}N - \frac{N^*}{\tau^*} - k_{\text{detrap}}N^* = 0 \tag{4}$$

where g (g^*) is the generation rate of excitons in the undecorated (decorated) state, N (N^*) is the exciton population in the undecorated (decorated) state, and τ (τ^*) is the lifetime of excitons in the undecorated (decorated) state. Under continuous-wave (CW) excitation, the generation rate and the recombination rate are considered equal, and the trapping and detrapping rates are sufficiently faster than exciton recombination as we have found from the PL decay curves. Hence, the terms containing g (g^*) and τ (τ^*) can be considered negligible, and the ratio between N^* and N is simply expressed as

$$\frac{N^*}{N} = \frac{k_{\text{trap}}}{k_{\text{detrap}}} \tag{5}$$

Experimentally, the exciton population ratio can be estimated by comparing the emission peak areas of the decorated peak and the undecorated peak. When we consider the PLE map taken at spot 4 in Figure 3(a), the peak area ratio $I^*/I = N^*/N \approx 1.4$. This value obtained from the emission peak area ratio is in reasonable agreement with the exciton population ratio 1.9 derived from the exciton trapping rate and the detrapping rate in eq 2, indicating that our trapping rate calculation is valid. The difference between the two values is likely caused by a lower emission quantum efficiency of the decorated peak which is not considered in this model. By comparing the two values, the decrease in the emission quantum efficiency due to pentacene decoration is estimated to be 26% in this CNT. Alternatively, discrepancy may also occur if the actual trapping and detrapping rates are not fast enough for g (g^*) and $1/\tau$ ($1/\tau^*$) to be negligible.

Additional time-resolved PL and photon correlation measurements are carried out on 8 more pentacene-decorated CNTs, where separate sets of data are acquired from the undecorated peak and the decorated peak (Supporting Table S1). No clear correlation can be found between the exciton lifetimes calculated from the undecorated and decorated peaks, again suggesting that the trapping and detrapping process is faster than exciton recombination. Meanwhile, values of $g^{(2)}(0)$ obtained at pulsed P = 20 nW from the undecorated peak and decorated peak are also compared. Various factors are known to have a potentially negative impact on the results, such as PL blinking, pentacene degradation over time, shortened exciton diffusion length limited by the thin molecular films in the undecorated region, as well as defocusing and misalignment due to occasional sample drifting. Nevertheless, clear antibunching is observed from both peaks, and 6 out of 8 CNTs exhibit a lower $g^{(2)}(0)$ from the decorated peak with a minimum value reaching 0.38. The average $g^{(2)}(0)$ from the decorated peak is also noticeably lower than that obtained from pristine air-suspended CNTs under a similar condition.[51] Moreover, after pentacene is removed by annealing, most of the values of $g^{(2)}(0)$ become greater than that from the decorated peak (Supporting Table S2), suggesting that the enhanced antibunching is indeed induced by the decorated pentacene particles. Overall, the decorated pentacene particles are generally beneficial for stronger photon antibunching in air-suspended CNTs.

CONCLUSIONS

In conclusion, we have demonstrated directional exciton transfer and room-temperature single-photon emission from air-suspended CNTs decorated with pentacene particles. Typical decorated pentacene particles have a diameter less than 100 nm, and the particle size can be controlled by adjusting the deposition parameters during thermal evaporation. Pentacene decoration is found to show a dependency on the CNT species, where CNTs with chiral angles larger than 20° are more likely to be decorated. CNTs are characterized by PL spectroscopy, and the typical depth of the potential well created by pentacene decoration is estimated to be less than 20 meV. The location of the decorated particle can be visualized in the PL image, and directional exciton transfer from the undecorated region to the decorated site is demonstrated in the PLE map where an additional 2u peak with redshifted E_{11} resonance emerges. Enhanced EEA induced by directional exciton transfer to the decorated site is confirmed in the representative CNT by excitation-power-dependent PL spectra, and the exciton trapping rate at the decorated site is estimated to be higher than the detrapping rate at room temperature. From photon correlation measurements, single-photon emission from the excitons in the decorated site is verified. More CNTs are also found to show enhance photon antibunching induced by pentacene decoration. To further modify the energy landscape, local laser heating can be adopted to pattern the distribution of the decorated particles. Moreover, a molecular type that can

https://doi.org/10.1021/acsphotonics.1c00539
ACS Photonics 2021, 8, 2367−2374

introduce deeper traps and cryogenic temperatures can be considered to give rise to an even lower $g^{(2)}(0)$. Our results indicate that noncovalent functionalization of CNTs using nanoscale molecular particles is a promising top-down approach for energy landscape modification and quantum emission at room temperature.

METHODS

Air-Suspended Carbon Nanotubes. Trenched Si/SiO_2 substrates are prepared before the synthesis of CNTs. Alignment markers along with trenches with a length of 900 μm and widths from 0.5 to 4 μm on Si substrates are patterned by electron-beam lithography followed by dry etching. A SiO_2 film with a thickness of 60−70 nm is then formed upon Si by thermal oxidation. An additional electron-beam lithography process defines the catalyst regions along the edge of the trenches. To synthesize air-suspended CNTs on such substrates, catalyst solution of iron acetylacetonate and fumed silica in ethanol is spin-coated onto the catalyst regions on the trenched Si/SiO_2 substrates followed by lift-off. CNTs are then grown across the trenches via alcohol chemical vapor deposition at 800 °C for 1 min.[26,72]

Pentacene Deposition. Substrates grown with air-suspended CNTs are loaded into a thermal evaporator chamber with a pressure on the order of 10^{-2} Pa. Then, pentacene powder (99%, Sigma-Aldrich) in an alumina crucible is heated by a tungsten filament using a current of 10 A with a typical deposition rate of 0.1−0.5 Å/s. Thickness of the deposited pentacene film on the substrates is monitored by a quartz crystal sensor during deposition.

Photoluminescence Spectroscopy. Before and after pentacene deposition, PL measurements are performed on the same air-suspended CNTs in a home-built confocal microscopy system.[26,51,61,70,73−75] A wavelength-tunable Ti:-sapphire laser with a CW output is used. The excitation laser beam with a power P and linear polarization parallel to the CNT axis is focused onto the sample by an objective lens with a numerical aperture of 0.8 and a focal length of 1.8 mm. The reflected beam and PL from the sample are collected by the same objective lens and separated by a dichroic mirror. A Si photodiode detects the reflected beam to visualize the trenches on the substrate, and PL is collected by an InGaAs photodiode array attached to a spectrometer.

Time-Resolved Measurements. For time-resolved PL and photon correlation measurements, a laser output of approximately 100 fs pulses and a repetition rate of 76 MHz is used. The excitation laser beam is focused onto the sample by an objective lens with a numerical aperture of 0.85 and a focal length of 1.8 mm. The data are collected by a fiber-coupled superconducting single-photon detector and a time-correlated single-photon counting module. Detection-wavelength-dependent IRFs are obtained by supercontinuum white light pulses dispersed by a spectrometer. Photon correlation measurements are carried out using a Hanbury-Brown-Twiss setup with a 50:50 fiber coupler. Unless otherwise noted, all measurements are carried out at room temperature in dry nitrogen to avoid degradation of pentacene.

ASSOCIATED CONTENT

Supporting Information

The Supporting Information is available free of charge at https://pubs.acs.org/doi/10.1021/acsphotonics.1c00539.

Transmission electron microscope images of pentacene-decorated CNTs, surface profiler scans of pentacene films on the sample substrate, method to obtain the percentage of pentacene-decorated CNTs, definition of the "pristine CNT", PLE maps of CNTs adsorbed with other polycyclic aromatic hydrocarbons, typical PL spectra with and without the bandpass filter, decay and $g^{(2)}(0)$ data from more pentacene-decorated CNTs, PL and $g^{(2)}(0)$ data after pentacene removal (PDF)

AUTHOR INFORMATION

Corresponding Authors

Zhen Li − *Quantum Optoelectronics Research Team, RIKEN Center for Advanced Photonics, Saitama 351-0198, Japan; Nanoscale Quantum Photonics Laboratory, RIKEN Cluster for Pioneering Research, Saitama 351-0198, Japan;* orcid.org/0000-0001-5195-8962; Email: zhen.li@riken.jp

Yuichiro K. Kato − *Quantum Optoelectronics Research Team, RIKEN Center for Advanced Photonics, Saitama 351-0198, Japan; Nanoscale Quantum Photonics Laboratory, RIKEN Cluster for Pioneering Research, Saitama 351-0198, Japan;* orcid.org/0000-0002-9942-1459; Email: yuichiro.kato@riken.jp

Authors

Keigo Otsuka − *Nanoscale Quantum Photonics Laboratory, RIKEN Cluster for Pioneering Research, Saitama 351-0198, Japan;* orcid.org/0000-0002-6694-0738

Daiki Yamashita − *Quantum Optoelectronics Research Team, RIKEN Center for Advanced Photonics, Saitama 351-0198, Japan;* orcid.org/0000-0002-6970-4677

Daichi Kozawa − *Quantum Optoelectronics Research Team, RIKEN Center for Advanced Photonics, Saitama 351-0198, Japan;* orcid.org/0000-0002-0629-5589

Complete contact information is available at: https://pubs.acs.org/10.1021/acsphotonics.1c00539

Notes

The authors declare no competing financial interest.

ACKNOWLEDGMENTS

This work is supported in part by MIC (SCOPE 191503001), JSPS (KAKENHI JP20H02558, JP19J00894, JP20J00817, JP20K15121, JP20K15137, JP20K15112, and JP20K15199), and MEXT (Nanotechnology Platform JPMXP09F19UT0079). K. O. and D. Y. are supported by the JSPS Research Fellowship. D. K. is supported by the RIKEN Special Postdoctoral Researcher Program. We acknowledge RIKEN Materials Characterization Team for access to the transmission electron microscope, and RIKEN Advanced Manufacturing Support Team for technical assistance.

REFERENCES

(1) O'Brien, J. L.; Furusawa, A.; Vučkovic, J. Photonic quantum technologies. *Nat. Photonics* **2009**, *3*, 687−695.

(2) Takemoto, K.; Nambu, Y.; Miyazawa, T.; Wakui, K.; Hirose, S.; Usuki, T.; Takatsu, M.; Yokoyama, N.; Yoshino, K.; Tomita, A.; Yorozu, S.; Sakuma, Y.; Arakawa, Y. Transmission Experiment of Quantum Keys over 50 km Using High-Performance Quantum-Dot Single-Photon Source at 1.5 μm Wavelength. *Appl. Phys. Express* **2010**, *3*, 092802.

(3) Aharonovich, I.; Englund, D.; Toth, M. Solid-state single-photon emitters. *Nat. Photonics* **2016**, *10*, 631−641.
(4) Senellart, P.; Solomon, G.; White, A. High-performance semiconductor quantum-dot single-photon sources. *Nat. Nanotechnol.* **2017**, *12*, 1026−1039.
(5) He, X.; Htoon, H.; Doorn, S. K.; Pernice, W. H. P.; Pyatkov, F.; Krupke, R.; Jeantet, A.; Chassagneux, Y.; Voisin, C. Carbon nanotubes as emerging quantum-light sources. *Nat. Mater.* **2018**, *17*, 663−670.
(6) Kimble, H. J.; Dagenais, M.; Mandel, L. Photon Antibunching in Resonance Fluorescence. *Phys. Rev. Lett.* **1977**, *39*, 691−695.
(7) Diedrich, F.; Walther, H. Nonclassical radiation of a single stored ion. *Phys. Rev. Lett.* **1987**, *58*, 203−206.
(8) Basché, T.; Moerner, W. E.; Orrit, M.; Talon, H. Photon antibunching in the fluorescence of a single dye molecule trapped in a solid. *Phys. Rev. Lett.* **1992**, *69*, 1516−1519.
(9) Lounis, B.; Moerner, W. E. Single photons on demand from a single molecule at room temperature. *Nature* **2000**, *407*, 491−493.
(10) Michler, P.; Imamoğlu, A.; Mason, M. D.; Carson, P. J.; Strouse, G. F.; Buratto, S. K. Quantum correlation among photons from a single quantum dot at room temperature. *Nature* **2000**, *406*, 968−970.
(11) Kurtsiefer, C.; Mayer, S.; Zarda, P.; Weinfurter, H. Stable Solid-State Source of Single Photons. *Phys. Rev. Lett.* **2000**, *85*, 290−293.
(12) Laurent, S.; Varoutsis, S.; Le Gratiet, L.; Lemaître, A.; Sagnes, I.; Raineri, F.; Levenson, A.; Robert-Philip, I.; Abram, I. Indistinguishable single photons from a single-quantum dot in a two-dimensional photonic crystal cavity. *Appl. Phys. Lett.* **2005**, *87*, 163107.
(13) Gazzano, O.; Michaelis de Vasconcellos, S.; Arnold, C.; Nowak, A.; Galopin, E.; Sagnes, I.; Lanco, L.; Lemaître, A.; Senellart, P. Bright solid-state sources of indistinguishable single photons. *Nat. Commun.* **2013**, *4*, 1425.
(14) Benyoucef, M.; Yacob, M.; Reithmaier, J. P.; Kettler, J.; Michler, P. Telecom-wavelength (1.5 μm) single-photon emission from InP-based quantum dots. *Appl. Phys. Lett.* **2013**, *103*, 162101.
(15) Choi, S.; Johnson, B. C.; Castelletto, S.; Ton-That, C.; Phillips, M. R.; Aharonovich, I. Single photon emission from ZnO nanoparticles. *Appl. Phys. Lett.* **2014**, *104*, 261101.
(16) Castelletto, S.; Johnson, B. C.; Ivády, V.; Stavrias, N.; Umeda, T.; Gali, A.; Ohshima, T. A silicon carbide room-temperature single-photon source. *Nat. Mater.* **2014**, *13*, 151−156.
(17) He, Y.-M.; Clark, G.; Schaibley, J. R.; He, Y.; Chen, M.-C.; Wei, Y.-J.; Ding, X.; Zhang, Q.; Yao, W.; Xu, X.; Lu, C.-Y.; Pan, J.-W. Single quantum emitters in monolayer semiconductors. *Nat. Nanotechnol.* **2015**, *10*, 497−502.
(18) Park, Y.-S.; Guo, S.; Makarov, N. S.; Klimov, V. I. Room Temperature Single-Photon Emission from Individual Perovskite Quantum Dots. *ACS Nano* **2015**, *9*, 10386−10393.
(19) Tran, T. T.; Bray, K.; Ford, M. J.; Toth, M.; Aharonovich, I. Quantum emission from hexagonal boron nitride monolayers. *Nat. Nanotechnol.* **2016**, *11*, 37−41.
(20) Zhou, Y.; Wang, Z.; Rasmita, A.; Kim, S.; Berhane, A.; Bodrog, Z.; Adamo, G.; Gali, A.; Aharonovich, I.; Gao, W.-b. Room temperature solid-state quantum emitters in the telecom range. *Sci. Adv.* **2018**, *4*, eaar3580.
(21) Wang, J.; Zhou, Y.; Wang, Z.; Rasmita, A.; Yang, J.; Li, X.; von Bardeleben, H. J.; Gao, W. Bright room temperature single photon source at telecom range in cubic silicon carbide. *Nat. Commun.* **2018**, *9*, 4106.
(22) Liu, F.; Brash, A. J.; O'Hara, J.; Martins, L. M. P. P.; Phillips, C. L.; Coles, R. J.; Royall, B.; Clarke, E.; Bentham, C.; Prtljaga, N.; Itskevich, I. E.; Wilson, L. R.; Skolnick, M. S.; Fox, A. M. High Purcell factor generation of indistinguishable on-chip single photons. *Nat. Nanotechnol.* **2018**, *13*, 835−840.
(23) Wang, F.; Dukovic, G.; Brus, L. E.; Heinz, T. F. The Optical Resonances in Carbon Nanotubes Arise from Excitons. *Science* **2005**, *308*, 838−841.
(24) Maultzsch, J.; Pomraenke, R.; Reich, S.; Chang, E.; Prezzi, D.; Ruini, A.; Molinari, E.; Strano, M. S.; Thomsen, C.; Lienau, C. Exciton binding energies in carbon nanotubes from two-photon photoluminescence. *Phys. Rev. B: Condens. Matter Mater. Phys.* **2005**, *72*, 241402.
(25) Weisman, R. B.; Bachilo, S. M. Dependence of Optical Transition Energies on Structure for Single-Walled Carbon Nanotubes in Aqueous Suspension: An Empirical Kataura Plot. *Nano Lett.* **2003**, *3*, 1235−1238.
(26) Ishii, A.; Yoshida, M.; Kato, Y. K. Exciton diffusion, end quenching, and exciton-exciton annihilation in individual air-suspended carbon nanotubes. *Phys. Rev. B: Condens. Matter Mater. Phys.* **2015**, *91*, 125427.
(27) Ogawa, T.; Takagahara, T. Optical absorption and Sommerfeld factors of one-dimensional semiconductors: An exact treatment of excitonic effects. *Phys. Rev. B: Condens. Matter Mater. Phys.* **1991**, *44*, 8138.
(28) Ando, T. Excitons in Carbon Nanotubes. *J. Phys. Soc. Jpn.* **1997**, *66*, 1066−1073.
(29) Cognet, L.; Tsyboulski, D. A.; Rocha, J.-D. R.; Doyle, C. D.; Tour, J. M.; Weisman, R. B. Stepwise Quenching of Exciton Fluorescence in Carbon Nanotubes by Single-Molecule Reactions. *Science* **2007**, *316*, 1465−1468.
(30) Lüer, L.; Hoseinkhani, S.; Polli, D.; Crochet, J.; Hertel, T.; Lanzani, G. Size and mobility of excitons in (6, 5) carbon nanotubes. *Nat. Phys.* **2009**, *5*, 54−58.
(31) Moritsubo, S.; Murai, T.; Shimada, T.; Murakami, Y.; Chiashi, S.; Maruyama, S.; Kato, Y. K. Exciton Diffusion in Air-Suspended Single-Walled Carbon Nanotubes. *Phys. Rev. Lett.* **2010**, *104*, 247402.
(32) Ma, X.; Roslyak, O.; Duque, J. G.; Pang, X.; Doorn, S. K.; Piryatinski, A.; Dunlap, D. H.; Htoon, H. Influences of Exciton Diffusion and Exciton-Exciton Annihilation on Photon Emission Statistics of Carbon Nanotubes. *Phys. Rev. Lett.* **2015**, *115*, 017401.
(33) Xie, J.; Inaba, T.; Sugiyama, R.; Homma, Y. Intrinsic diffusion length of excitons in long single-walled carbon nanotubes from photoluminescence spectra. *Phys. Rev. B: Condens. Matter Mater. Phys.* **2012**, *85*, 085434.
(34) Ghosh, S.; Bachilo, S. M.; Simonette, R. A.; Beckingham, K. M.; Weisman, R. B. Oxygen Doping Modifies Near-Infrared Band Gaps in Fluorescent Single-Walled Carbon Nanotubes. *Science* **2010**, *330*, 1656−1659.
(35) Miyauchi, Y.; Iwamura, M.; Mouri, S.; Kawazoe, T.; Ohtsu, M.; Matsuda, K. Brightening of excitons in carbon nanotubes on dimensionality modification. *Nat. Photonics* **2013**, *7*, 715−719.
(36) Piao, Y.; Meany, B.; Powell, L. R.; Valley, N.; Kwon, H.; Schatz, G. C.; Wang, Y. Brightening of carbon nanotube photoluminescence through the incorporation of sp^3 defects. *Nat. Chem.* **2013**, *5*, 840−845.
(37) Ma, X.; Adamska, L.; Yamaguchi, H.; Yalcin, S. E.; Tretiak, S.; Doorn, S. K.; Htoon, H. Electronic Structure and Chemical Nature of Oxygen Dopant States in Carbon Nanotubes. *ACS Nano* **2014**, *8*, 10782−10789.
(38) Ma, X.; Hartmann, N. F.; Baldwin, J. K. S.; Doorn, S. K.; Htoon, H. Room-temperature single-photon generation from solitary dopants of carbon nanotubes. *Nat. Nanotechnol.* **2015**, *10*, 671−675.
(39) He, X.; Hartmann, N. F.; Ma, X.; Kim, Y.; Ihly, R.; Blackburn, J. L.; Gao, W.; Kono, J.; Yomogida, Y.; Hirano, A.; Tanaka, T.; Kataura, H.; Htoon, H.; Doorn, S. K. Tunable room-temperature single-photon emission at telecom wavelengths from sp^3 defects in carbon nanotubes. *Nat. Photonics* **2017**, *11*, 577−582.
(40) Ishii, A.; He, X.; Hartmann, N. F.; Machiya, H.; Htoon, H.; Doorn, S. K.; Kato, Y. K. Enhanced Single-Photon Emission from Carbon-Nanotube Dopant States Coupled to Silicon Microcavities. *Nano Lett.* **2018**, *18*, 3873−3878.
(41) Htoon, H.; O'Connell, M. J.; Cox, P. J.; Doorn, S. K.; Klimov, V. I. Low Temperature Emission Spectra of Individual Single-Walled Carbon Nanotubes: Multiplicity of Subspecies within Single-Species Nanotube Ensembles. *Phys. Rev. Lett.* **2004**, *93*, 027401.
(42) Hirori, H.; Matsuda, K.; Miyauchi, Y.; Maruyama, S.; Kanemitsu, Y. Exciton Localization of Single-Walled Carbon Nano-

https://doi.org/10.1021/acsphotonics.1c00539
ACS Photonics 2021, 8, 2367−2374

tubes Revealed by Femtosecond Excitation Correlation Spectroscopy. *Phys. Rev. Lett.* **2006**, *97*, 257401.
(43) Högele, A.; Galland, C.; Winger, M.; Imamoğlu, A. Photon Antibunching in the Photoluminescence Spectra of a Single Carbon Nanotube. *Phys. Rev. Lett.* **2008**, *100*, 217401.
(44) Walden-Newman, W.; Sarpkaya, I.; Strauf, S. Quantum Light Signatures and Nanosecond Spectral Diffusion from Cavity-Embedded Carbon Nanotubes. *Nano Lett.* **2012**, *12*, 1934−1941.
(45) Hofmann, M. S.; Glückert, J. T.; Noé, J.; Bourjau, C.; Dehmel, R.; Högele, A. Bright, long-lived and coherent excitons in carbon nanotube quantum dots. *Nat. Nanotechnol.* **2013**, *8*, 502−505.
(46) Sarpkaya, I.; Zhang, Z.; Walden-Newman, W.; Wang, X.; Hone, J.; Wong, C. W.; Strauf, S. Prolonged spontaneous emission and dephasing of localized excitons in air-bridged carbon nanotubes. *Nat. Commun.* **2013**, *4*, 2152.
(47) Vialla, F.; Chassagneux, Y.; Ferreira, R.; Roquelet, C.; Diederichs, C.; Cassabois, G.; Roussignol, P.; Lauret, J. S.; Voisin, C. Unifying the Low-Temperature Photoluminescence Spectra of Carbon Nanotubes: The Role of Acoustic Phonon Confinement. *Phys. Rev. Lett.* **2014**, *113*, 057402.
(48) Endo, T.; Ishi-Hayase, J.; Maki, H. Photon antibunching in single-walled carbon nanotubes at telecommunication wavelengths and room temperature. *Appl. Phys. Lett.* **2015**, *106*, 113106.
(49) Hofmann, M. S.; Noé, J.; Kneer, A.; Crochet, J. J.; Högele, A. Ubiquity of Exciton Localization in Cryogenic Carbon Nanotubes. *Nano Lett.* **2016**, *16*, 2958−2962.
(50) Raynaud, C.; Claude, T.; Borel, A.; Amara, M. R.; Graf, A.; Zaumseil, J.; Lauret, J.-S.; Chassagneux, Y.; Voisin, C. Super-localization of Excitons in Carbon Nanotubes at Cryogenic Temperature. *Nano Lett.* **2019**, *19*, 7210−7216.
(51) Ishii, A.; Uda, T.; Kato, Y. K. Room-Temperature Single-Photon Emission from Micrometer-Long Air-Suspended Carbon Nanotubes. *Phys. Rev. Appl.* **2017**, *8*, 054039.
(52) Lefebvre, J.; Fraser, J. M.; Homma, Y.; Finnie, P. Photoluminescence from single-walled carbon nanotubes: a comparison between suspended and micelle-encapsulated nanotubes. *Appl. Phys. A: Mater. Sci. Process.* **2004**, *78*, 1107−1110.
(53) Finnie, P.; Homma, Y.; Lefebvre, J. Band-Gap Shift Transition in the Photoluminescence of Single-Walled Carbon Nanotubes. *Phys. Rev. Lett.* **2005**, *94*, 247401.
(54) Milkie, D. E.; Staii, C.; Paulson, S.; Hindman, E.; Johnson, A. T.; Kikkawa, J. M. Controlled Switching of Optical Emission Energies in Semiconducting Single-Walled Carbon Nanotubes. *Nano Lett.* **2005**, *5*, 1135−1138.
(55) Ohno, Y.; Iwasaki, S.; Murakami, Y.; Kishimoto, S.; Maruyama, S.; Mizutani, T. Chirality-dependent environmental effects in photoluminescence of single-walled carbon nanotubes. *Phys. Rev. B: Condens. Matter Mater. Phys.* **2006**, *73*, 235427.
(56) Homma, Y.; Chiashi, S.; Yamamoto, T.; Kono, K.; Matsumoto, D.; Shitaba, J.; Sato, S. Photoluminescence Measurements and Molecular Dynamics Simulations of Water Adsorption on the Hydrophobic Surface of a Carbon Nanotube in Water Vapor. *Phys. Rev. Lett.* **2013**, *110*, 157402.
(57) Uda, T.; Ishii, A.; Kato, Y. K. Single Carbon Nanotubes as Ultrasmall All-Optical Memories. *ACS Photonics* **2018**, *5*, 559−565.
(58) Machiya, H.; Uda, T.; Ishii, A.; Kato, Y. K. Spectral tuning of optical coupling between air-mode nanobeam cavities and individual carbon nanotubes. *Appl. Phys. Lett.* **2018**, *112*, 021101.
(59) Uda, T.; Tanaka, S.; Kato, Y. K. Molecular screening effects on exciton-carrier interactions in suspended carbon nanotubes. *Appl. Phys. Lett.* **2018**, *113*, 121105.
(60) Tanaka, S.; Otsuka, K.; Kimura, K.; Ishii, A.; Imada, H.; Kim, Y.; Kato, Y. K. Organic Molecular Tuning of Many-Body Interaction Energies in Air-Suspended Carbon Nanotubes. *J. Phys. Chem. C* **2019**, *123*, 5776−5781.
(61) Fang, N.; Otsuka, K.; Ishii, A.; Taniguchi, T.; Watanabe, K.; Nagashio, K.; Kato, Y. K. Hexagonal Boron Nitride As an Ideal Substrate for Carbon Nanotube Photonics. *ACS Photonics* **2020**, *7*, 1773−1779.
(62) Dimitrakopoulos, C.; Malenfant, P. Organic Thin Film Transistors for Large Area Electronics. *Adv. Mater.* **2002**, *14*, 99−117.
(63) Knipp, D.; Street, R. A.; Völkel, A.; Ho, J. Pentacene thin film transistors on inorganic dielectrics: Morphology, structural properties, and electronic transport. *J. Appl. Phys.* **2003**, *93*, 347−355.
(64) Ruiz, R.; Choudhary, D.; Nickel, B.; Toccoli, T.; Chang, K.-C.; Mayer, A. C.; Clancy, P.; Blakely, J. M.; Headrick, R. L.; Iannotta, S.; Malliaras, G. G. Pentacene Thin Film Growth. *Chem. Mater.* **2004**, *16*, 4497−4508.
(65) Virkar, A. A.; Mannsfeld, S.; Bao, Z.; Stingelin, N. Organic Semiconductor Growth and Morphology Considerations for Organic Thin-Film Transistors. *Adv. Mater.* **2010**, *22*, 3857−3875.
(66) Liu, C.-H.; Liu, Y.-Y.; Zhang, Y.-H.; Wei, R.-R.; Zhang, H.-L. Tandem extraction strategy for separation of metallic and semiconducting SWCNTs using condensed benzenoid molecules: effects of molecular morphology and solvent. *Phys. Chem. Chem. Phys.* **2009**, *11*, 7257−7267.
(67) Lefebvre, J.; Finnie, P. Excited Excitonic States in Single-Walled Carbon Nanotubes. *Nano Lett.* **2008**, *8*, 1890−1895.
(68) Mortimer, I. B.; Nicholas, R. J. Role of Bright and Dark Excitons in the Temperature-Dependent Photoluminescence of Carbon Nanotubes. *Phys. Rev. Lett.* **2007**, *98*, 027404.
(69) Berciaud, S.; Cognet, L.; Lounis, B. Luminescence Decay and the Absorption Cross Section of Individual Single-Walled Carbon Nanotubes. *Phys. Rev. Lett.* **2008**, *101*, 077402.
(70) Ishii, A.; Machiya, H.; Kato, Y. High Efficiency Dark-to-Bright Exciton Conversion in Carbon Nanotubes. *Phys. Rev. X* **2019**, *9*, 041048.
(71) Sykes, M. E.; Kim, M.; Wu, X.; Wiederrecht, G. P.; Peng, L.; Wang, Y.; Gosztola, D. J.; Ma, X. Ultrafast Exciton Trapping at sp3 Quantum Defects in Carbon Nanotubes. *ACS Nano* **2019**, *13*, 13264−13270.
(72) Maruyama, S.; Kojima, R.; Miyauchi, Y.; Chiashi, S.; Kohno, M. Low-Temperature Synthesis of High-Purity Single-Walled Carbon Nanotubes from Alcohol. *Chem. Phys. Lett.* **2002**, *360*, 229−234.
(73) Watahiki, R.; Shimada, T.; Zhao, P.; Chiashi, S.; Iwamoto, S.; Arakawa, Y.; Maruyama, S.; Kato, Y. K. Enhancement of Carbon Nanotube Photoluminescence by Photonic Crystal Nanocavities. *Appl. Phys. Lett.* **2012**, *101*, 141124.
(74) Jiang, M.; Kumamoto, Y.; Ishii, A.; Yoshida, M.; Shimada, T.; Kato, Y. K. Gate-controlled generation of optical pulse trains using individual carbon nanotubes. *Nat. Commun.* **2015**, *6*, 6335.
(75) Otsuka, K.; Ishii, A.; Kato, Y. K. Super-resolution fluorescence imaging of carbon nanotubes using a nonlinear excitonic process. *Opt. Express* **2019**, *27*, 17463.

https://doi.org/10.1021/acsphotonics.1c00539
ACS Photonics 2021, 8, 2367−2374